Aerodynamic Performance of an Annular Flat Plate Airfoil Cascade with Nonuniform Inlet Velocity

Daniel Buffum* and Sanford Fleeter†
Purdue University, West Lafayette, Indiana

The demand for increased gas turbine engine efficiency with minimum weight is leading to more complex blading designs, in which viscous and three-dimensional effects are significant. As a result, design procedures based on first principle, experimentally verified, three-dimensional aerodynamic analyses are required. This paper describes a series of experiments performed in a large-scale, subsonic, annular cascade facility specifically designed to provide three-dimensional aerodynamic data suitable for code verification. In particular, the effect of inlet velocity profile on the overall three-dimensional performance of a classical flat plate airfoil cascade is investigated over a range of incidence angles including those resulting in airfoil surface flow separation. All of the data are analyzed and correlated with appropriate nonseparated flow predictions.

Nomenclature

C_p = airfoil surface pressure coefficient
$L_{1/2}$ = wake half-width
P_{af} = airfoil surface static pressure
P_{Tfs} = freestream total pressure
P_{T1} = mass-averaged inlet total pressure
P_{T2} = exit total pressure
R = normalized radial position
S = airfoil spacing
T = tangential coordinate axis, tangential position
U = velocity magnitude
U_{fs} = average freestream velocity
U_i = circumferentially averaged rake velocities
U_0 = mass-averaged inlet velocity
W = velocity deficit
W_{CL} = airfoil centerline velocity deficit
Z = axial coordinate axis
η = normalized tangential distance, $T/L_{1/2}$
ρ_0 = inlet fluid density

Subscripts

R = radial component
T = tangential component
Z = axial component

I. Introduction

THE demand for increased gas turbine engine efficiency with minimum weight is leading to more complex compressor and turbine blading designs. Present designs rely heavily upon two-dimensional data obtained from airfoil cascades that are geometrically similar to rotor and stator airfoil sections. However, as stage loadings increase and blading aspect ratios decrease, viscous and three-dimensional effects become increasingly significant.[1,2] Furthermore, inviscid flow solvers now allow the design of complex airfoil shapes—which are not of geometric families for which test data exist—with optimum pressure distributions and attached boundary layers.[3] As a result, the traditional semiempirical two-dimensional design approach for turbomachinery blading is becoming inadequate, with procedures based on first principle, experimentally verified, three-dimensional aerodynamic analyses required.

Three-dimensional viscous and inviscid numerical analyses are currently being developed to predict the complex flow through turbomachine blade passages. Of necessity, these analyses involve many numerical and physical assumptions. To evaluate these analyses, predictions are currently correlated with data obtained from experiments involving flow through curved ducts and tubes, per Refs. 4 and 5, for example. To be of value to the designer, however, these numerical solutions must be experimentally evaluated by correlating predicted flowfields with data obtained from experiments that model the fundamental three-dimensional flow phenomena inherent in turbomachine blade rows, including flow separation.

This paper describes a series of experiments performed in a large-scale, subsonic, annular cascade facility specifically designed to provide three-dimensional aerodynamic data suitable for code verification. In particular, these experiments consider the effect of inlet velocity profile, i.e., potential and rotational flowfields, on the overall three-dimensional aerodynamic performance of a classical flat plate airfoil cascade over a range of incidence angles including those resulting in airfoil surface flow separation. All of these data are correlated with appropriate nonseparated flow predictions.

II. Annular Cascade Facility

The Purdue Annular Cascade Facility, depicted schematically in Fig. 1, was designed specifically to investigate fundamental three-dimensional turbomachinery flowfields.

Following the flow from left to right, the air enters a bellmouth section, which serves to accelerate the flow smoothly into an annular section 15.24 cm (6.0 in.) in span, which is maintained through the exit region of the facility.

Rakes of stagnation tubes, equispaced circumferentially, span the annulus to provide inlet velocity measurements. Each rake has 10 total pressure taps, radially distributed such that each tap is located at the center of a concentric, equal area, annulus. In addition, a set of static pressure taps is located in the outer shroud adjacent to each rake, thereby permitting determination of the cascade inlet velocity profile.

Presented as Paper 84-0619 at the AIAA 13th Aerodynamic Testing Conference, San Diego, CA, March 5-7, 1984; received June 26, 1984; revision received Feb. 5, 1985.

*Graduate Research Assistant, School of Mechanical Engineering.
†Professor, School of Mechanical Engineering; Director, Thermal Sciences and Propulsion Center. Associate Fellow AIAA.

Thirty-six airfoils are mounted in the test section. As the inlet flowfield is axial, the incidence angle is established by rotating the airfoils. Downstream of the airfoils are two circumferential traversing slots. These allow probe insertion into the test section and permit full radial and 45-deg circumferential traverses of the annulus. The probe positioning accuracy is ±0.23 deg, ±0.01 cm, and ±0.018 deg for the circumferential, radial, and self-rotational motions, respectively.

As the flow exits the facility, it undergoes a sudden expansion into a plenum chamber. Having a volume of 24 m^3 (850 ft^3, the chamber provides a uniform cascade exit pressure. The plenum chamber is connected to a centrifugal blower rated to deliver 354 cm/s (150,000 ft^3/min) of air at 46 cm (18 in.) of water pressure differential, with power provided by a 224 kW (300 hp) three-phase induction motor.

III. Experiment Design and Instrumentation

The cascade inlet velocity profile is nominally uniform. Thus, inlet profile generation screens were fabricated to vary the inlet profile. Each screen has a support of 16-mesh screening, then sheets of 100-mesh screening layered on top. By varying the number of layers and the width of the individual portions, the screens were tailored to create the desired profiles.

To provide data suitable for code verification while minimizing the complications associated with complex airfoil profiles, an instrumented classical airfoil cascade was designed and fabricated. The flat plate airfoils have rounded leading and trailing edges, a unity aspect ratio, a chord of 15.24 cm (6.0 in.), and a thickness-to-chord ratio of 3.15%. The midspan cascade characteristics and the nominal experimental conditions are presented in Table 1.

To distribute the airfoil surface static pressure taps such that there is a higher density over the front and rear portions of the airfoil, a Gauss-Legendre array of surface static taps was installed on the 10, 50, and 90% span streamlines of the airfoils.

For three-dimensional mean velocity measurements in the exit region of the cascade, a five-port cone probe operated in the nonnulling mode was used.[7] Bryer and Pankhurst[8] concluded that for pitch and yaw angles of less than 25 deg, this type of probe was accurate to ±3%. Sitaram, Lakshminarayana, and Ravindranath[9] found that the effect of flow acceleration between the probe and the wall was negligible when the probe was more than 2 diam from the wall and that, for turbulence intensities of up to 10%, the velocity error was 0.33%. In the present study, intensities in the wake region were typically found to be less than 10%.

In the aft region of the airfoil passage, a single slanted hot-wire probe aligned in the axial direction was used to measure the flowfield. A gearbox assembly was used to transform a self-rotation motion of the traversing system into rotation of the hot-wire probe about its own stem, a feature required for the three-dimensional, single slanted hot-wire technique utilized in these experiments.[10]

Table 1 Cascade geometry and experimental conditions

Tip diameter, cm	127.0
Hub/tip radius ratio	0.76
Airfoil span, cm	15.24
Cascade tip solidity	1.38
Number of airfoils	36
Airfoil type	Flat plate
Airfoil chord, cm	15.24
Axial velocity, m/s	29.0
Flow rate, m^3/s	15.5
Chord Reynolds number	300,000

IV. Data Acquisition and Reduction

The data acquisition and reduction system is centered on a computer-controlled data acquisition unit that permits automated probe positioning, data acquisition, and on-line data reduction and examination.

Pressure data are utilized to determine the cascade inlet velocity profile, the airfoil surface pressure distributions, and the cascade exit region flowfield. All of these measurements are accomplished utilizing a Scanivalve system controlled by the data acquisition system. As an integral part of the scanning procedure, the transducers are calibrated each time they are used. Also, statistical techniques have been incorporated into the software to permit confidence intervals to be placed on the data. A standard root-mean-square error analysis technique[11] was applied to these pressure data, with measurement errors taken as the statistical 99% confidence t-test values calculated for each sampling. Errors in the total and static measurements were less than 1%, while velocity data errors were less than 5%.

The inlet velocity profiles are determined from the inlet total pressure rakes and shroud static pressure taps via the isentropic flow relations.

The airfoil surface static pressure data are analyzed in the form of the dimensionless pressure coefficient

$$C_p = \frac{P_{Tfs} - P_{af}}{\frac{1}{2}\rho_0 U_0^2} \tag{1}$$

At each radial position, the cascade exit region data were determined via the cone probe in sets of 25 circumferential measurement stations. Figure 2 presents these stations, together with the cascade geometry and nomenclature. These pressure data were analyzed to determine the circumferential variation of 1) the absolute velocity U and the axial, tangential, and radial velocity components U_Z, U_T, and U_R, defined relative to the cascade coordinate system (Fig. 1); 2) the total pressure recovery, P_{T2}/P_{T1}; and 3) the exit flow angle, which is the angle between the absolute velocity and axial.

An automated data acquisition and reduction routine was also utilized for the hot-wire three-dimensional mean velocity measurements. At each radial location, the probe was

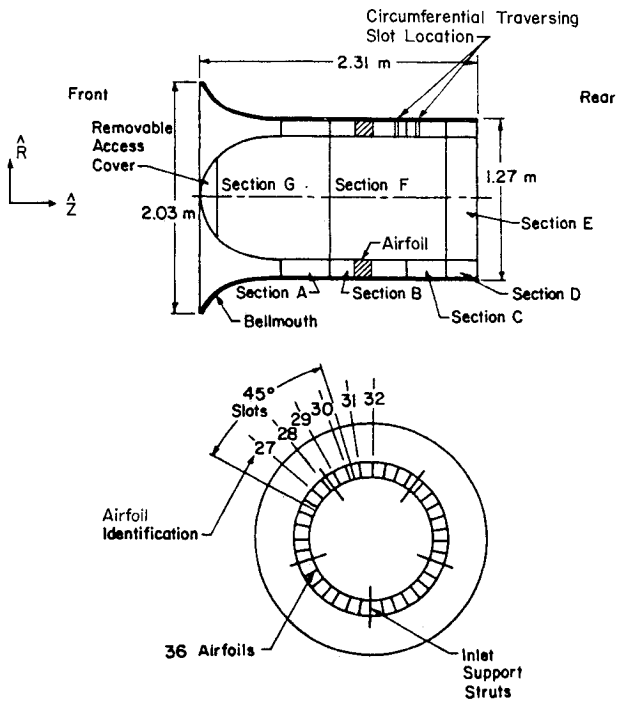

Fig. 1 Schematic of the Purdue Annular Cascade Facility.

Station	T (deg)	2T/S	Station	T (deg)	2T/S
1	-5.0	-1.00	14	0.25	0.05
2	-4.25	-0.85	15	0.5	0.10
3	-3.5	-0.70	16	0.75	0.15
4	-2.75	-0.55	17	1.0	0.20
5	-2.0	-0.40	18	1.25	0.25
6	-1.75	-0.35	19	1.5	0.30
7	-1.5	-0.30	20	1.75	0.35
8	-1.25	-0.25	21	2.0	0.40
9	-1.0	-0.20	22	2.75	0.55
10	-0.75	-0.15	23	3.5	0.70
11	-0.5	-0.10	24	4.25	0.85
12	-0.25	-0.05	25	5.0	1.00
13	0.0	0.00			

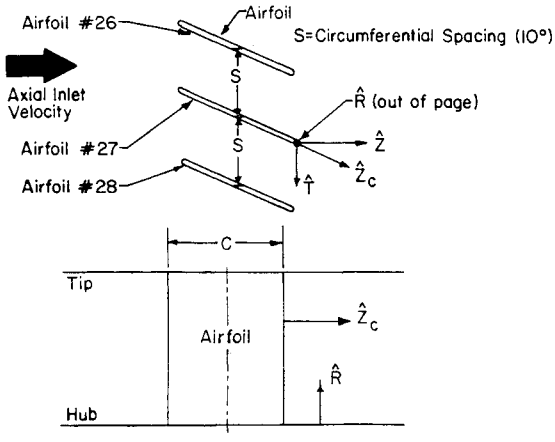

Fig. 2 Circumferential cascade geometry and nomenclature.

automatically traversed circumferentially to preset positions. At each measurement station, the anemometer output was sampled at three self-rotation positions, and solutions to the resulting set of response equations obtained. The number of samples was determined statistically by the acquisition software based on the fluctuations of the anemometer output. Sufficient samples were acquired such that with a 95% confidence interval for U_{eff}, the error is less than 1%.

V. Results

Inlet Velocity Profiles

The cascade inlet hub-peaked, uniform, and tip-peaked radial velocity profiles are shown in Fig. 3. The individual rake velocities are circumferentially averaged at each radial position to determine U_i, and then normalized with respect to the appropriate mass-averaged inlet velocity U_0. For the hub-peaked profile, the maximum velocity is approximately 27% greater than the mass-averaged velocity. This hub-peaked region extends radially from the hub to approximately midspan, and then remains nearly uniform radially outward to the tip. The maximum velocity for the tip-peaked profile is about 20% greater than the corresponding mass-averaged velocity. This tip-peaked region extends radially from the tip to approximately midspan and then slightly increases as the hub is approached.

Airfoil Surface Pressure Distributions

The chordwise airfoil surface dimensionless pressure coefficients C_p are presented with 99% confidence intervals indicated by bars and correlated with predictions obtained from the NASA numerical programs MERIDL[12] and TSONIC[13].

MERIDL and TSONIC generate a quasi-three-dimensional solution for the inviscid flow through an airfoil cascade via solution of the governing equations on intersecting stream surfaces. MERIDL solves for the hub-to-tip stream surface flow.

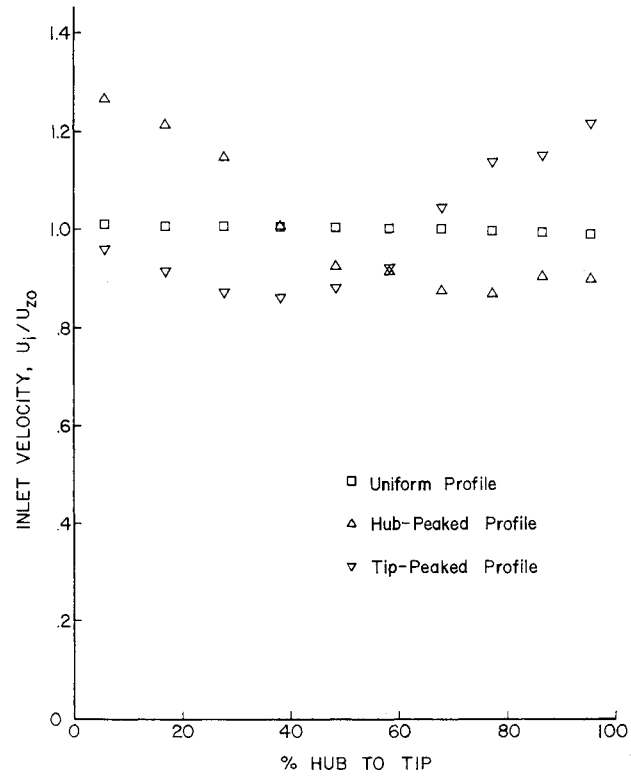

Fig. 3 Inlet velocity profile.

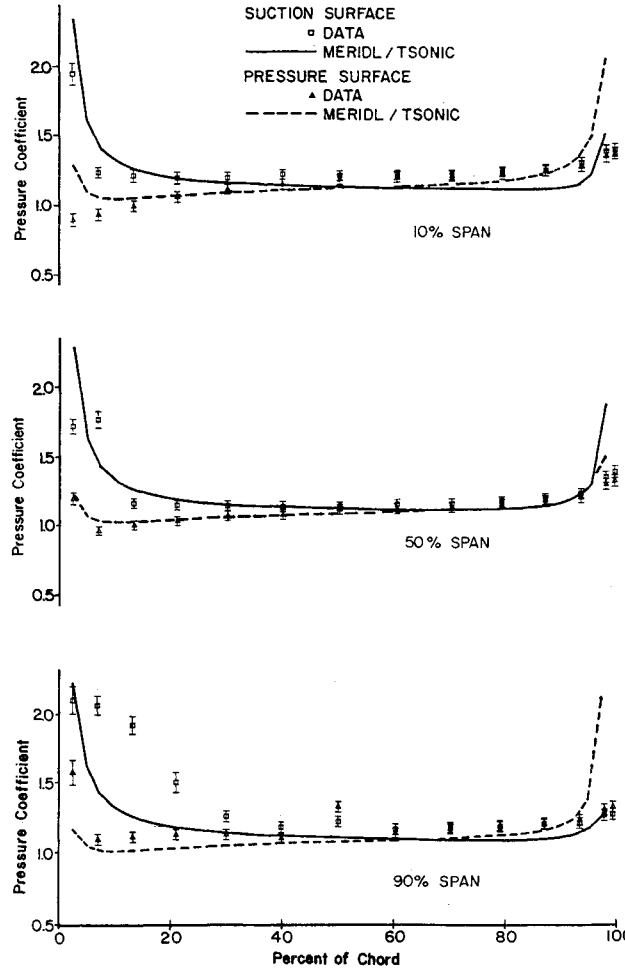

Fig. 4 Airfoil surface static pressure data-theory correlation at 5 deg of incidence with a uniform inlet.

This solution provides boundary conditions for TSONIC, which then calculates the airfoil-to-airfoil stream surface flowfield. The MERIDL calculations were performed on a 20×40 midchannel mesh; 20 mesh points spanned the passage from hub-to-tip, and 40 points were used in the streamwise direction. Thirty of the streamwise points were concentrated in a region extending from 10% of a chord length upstream of the leading edge to 10% of a chord length downstream of the trailing edge. A 20×81 mesh was used for TSONIC calculations, 81 points being used in the streamwise direction. TSONIC calculations were obtained at 10, 50, and 90% of span, thus coinciding with the chordwise arrays of airfoil static pressure taps.

At 5 deg of incidence with a uniform inlet velocity profile (Fig. 4), the trendwise agreement between the airfoil surface pressure coefficient data and the MERIDL/TSONIC predictions is generally good. At midspan, a leading-edge suction surface flow separation is apparent, as indicated by the constant static pressure. As expected, this separation is not predicted by the inviscid numerical codes. Also, the data exhibit sharper gradients at the leading edge of the pressure surface than the predictions, possibly due to a smoothing effect in the numerical analysis. The somewhat poor correlation in the trailing-edge region is attributed to the airfoil surface boundary layers and the possibility of trailing-edge separation. On both the suction and pressure surfaces, the deviations between the data and the predictions gradually increase along the aft part of the airfoil chord. This is also due to boundary-layer development, which is neglected in the inviscid codes. At approximately 60% chord, the suction and pressure surface C_p values become equal and remain nearly constant over the remainder of the chord.

At 10% span, in the leading edge region (Fig. 4), the suction surface does not appear to be separated nor does there appear to be a peak in the minimum value of the pressure surface C_p value. Also, the suction and pressure surface C_p values become equal in value near midchord, but do not remain constant or equal aft of this location. These differences between the 10% span and the midspan results are possibly due to the three-dimensionality of the flowfield and the interactions of the 10% span with the inner shroud boundary layer. Measurements of the annulus velocity profile at the position of the airfoil leading edge indicate the hub boundary layer extends to approximately 10% span.

The 90% span data are presented in Fig. 4. At the leading edge, suction surface separation is evident, while a peak exists on the pressure surface. In general, the experimental coefficients are larger than the predicted ones, except in the trailing-edge region.

At 10 deg of incidence, the quantitative agreement between the data and the numerical predictions for the three inlet velocity profiles is generally poor, as expected. This is demonstrated for the uniform inlet in Fig. 5. The midspan and tip region data indicate large regions of suction surface flow separation which, as expected, the inviscid codes do not predict. The suction surface flow appears to be attached in the hub region. Similar trends were noted at 5 deg of incidence: separation is evident at the midspan and tip locations but not at the hub.

Aft-Passage Region Flowfield

Figures 6 through 10 demonstrate the effect of inlet velocity profile on the aft-passage region flowfield. Per Fig. 2, a normalized tangential position of $2T/S = -2$ defines the pressure surface of one airfoil, with the suction surface of the adjacent airfoil defined by $2T/S = 0$. These velocity data are normalized with the average freestream velocity U_{fs}. Data were acquired circumferentially near the airfoil suction surface. However, due to probe interference effects, analogous data could not be obtained circumferentially close to the pressure surface.

Figures 6 and 7 present the 5-deg incidence aft-passage region dimensionless axial, tangential, and radial velocity

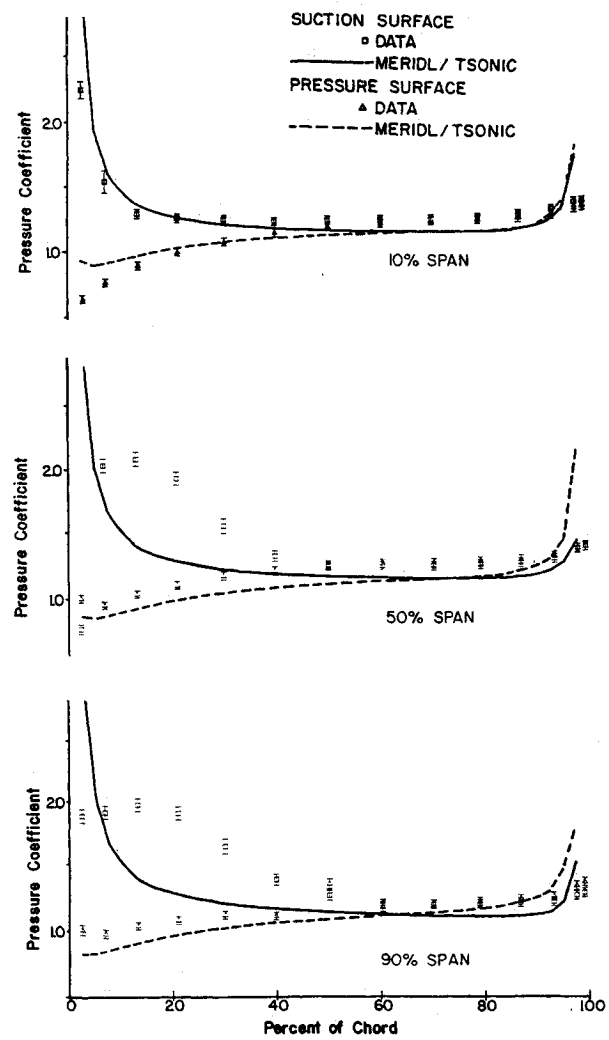

Fig. 5 Airfoil surface static pressure data-theory correlation at 10 deg of incidence with a uniform inlet.

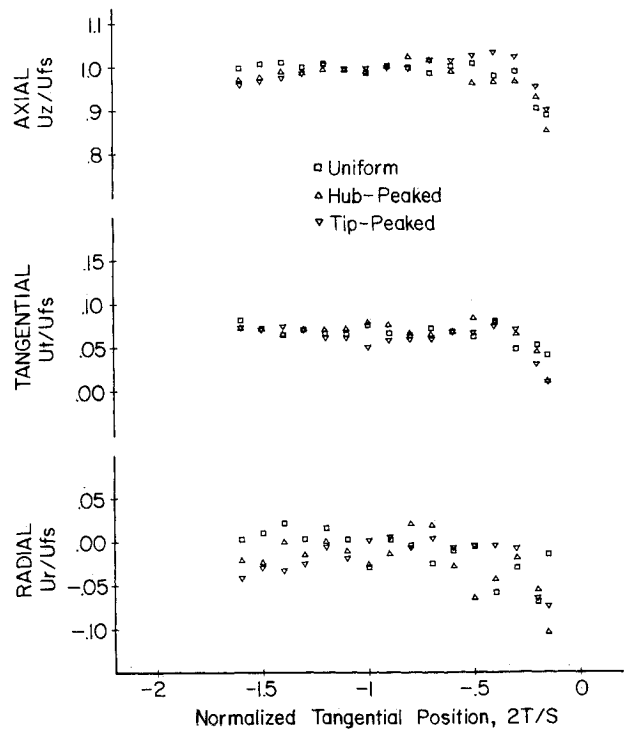

Fig. 6 Aft-passage velocity distributions at $R = 16.7\%$ at 5 deg of incidence.

component data at the 16.7% and 33.3% span locations, respectively. As seen, the axial and tangential distributions are relatively smooth, with the freestream and suction surface boundary-layer regions clearly visible. No distinctive trends with inlet velocity profile are apparent for these two velocity components, although at 16.7% span the pressure surface appears to have some influence on the axial velocity data for the hub- and tip-peaked inlet profiles at $2T/S = -1.5$, a circumferential distance equal to 25% of the airfoil passage. At 33.3% span, this pressure surface effect is still apparent for the hub-peaked inlet profile.

Radial flow toward the airfoil pressure surface is apparent at a circumferential distance of at least 25% of the passage ($2T/S = -1.5$) for both the hub- and tip-peaked inlet profiles at 16.7% span and for the hub-peaked profile at 33.3% span. The uniform inlet data exhibit no radial flow toward the airfoil pressure surface at the circumferential positions considered. The radial flow toward the airfoil suction surface is confined to a region extending over about 15% of the passage, with no variation with inlet profile apparent at 33.3% span. These radial velocity data exhibit increased scatter, as compared to the axial and tangential velocity data, with this scatter being larger nearer to the hub (<16.7% span). This is associated with the relatively small velocity magnitudes being measured.

Figures 8-10 demonstrate the effect of incidence angle on the aft-passage region axial velocity data at the 16.7, 25, and 50% span positions for the three inlet velocity profiles. In all cases, the circumferential variation of the data is relatively smooth, with the suction surface boundary-layer and freestream regions clearly evident.

With a uniform inlet (Fig. 8), no flow separation is evident at 5 deg of incidence. However, at 10 deg, some suction surface flow separation is apparent at 16.7% span. At 25 and 50% span, this 10-deg suction surface flow separation is clearly visible.

Analogous results are apparent for the tip-peaked inlet velocity profile data (Fig. 9). The 5-deg incidence angle data do not appear to be separated, whereas there is evidence of some suction surface separation at 16.7%, with this separated region becoming larger at 25 and 50%.

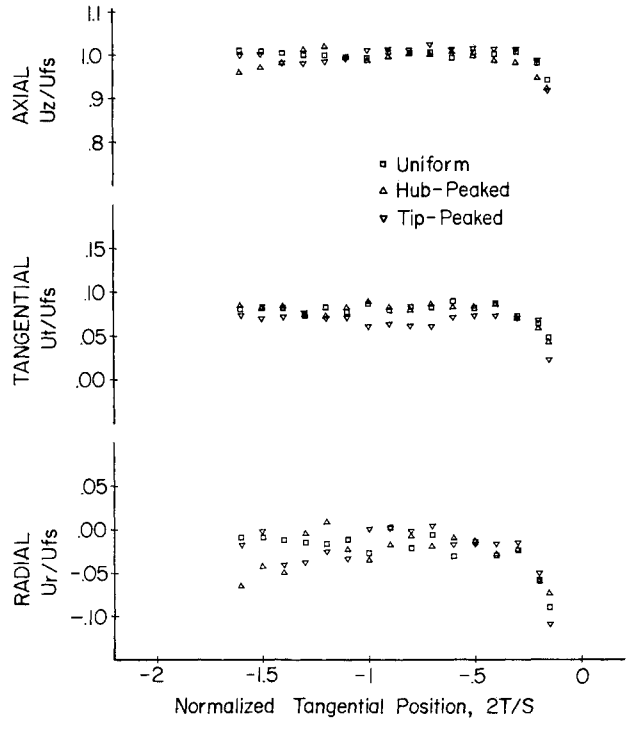

Fig. 7 Aft-passage velocity distributions at $R = 33.3\%$ at 5 deg of incidence.

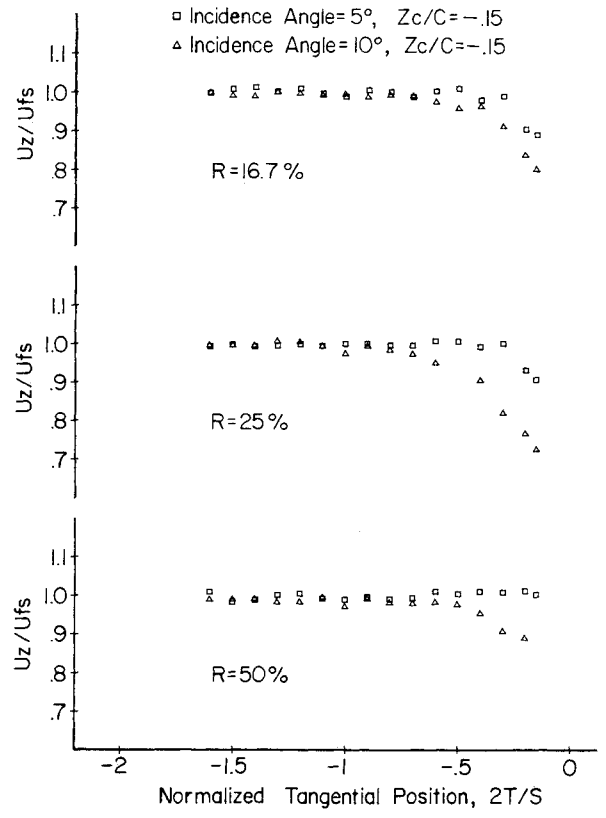

Fig. 8 Variation of the aft-passage axial velocity with incidence for a uniform inlet.

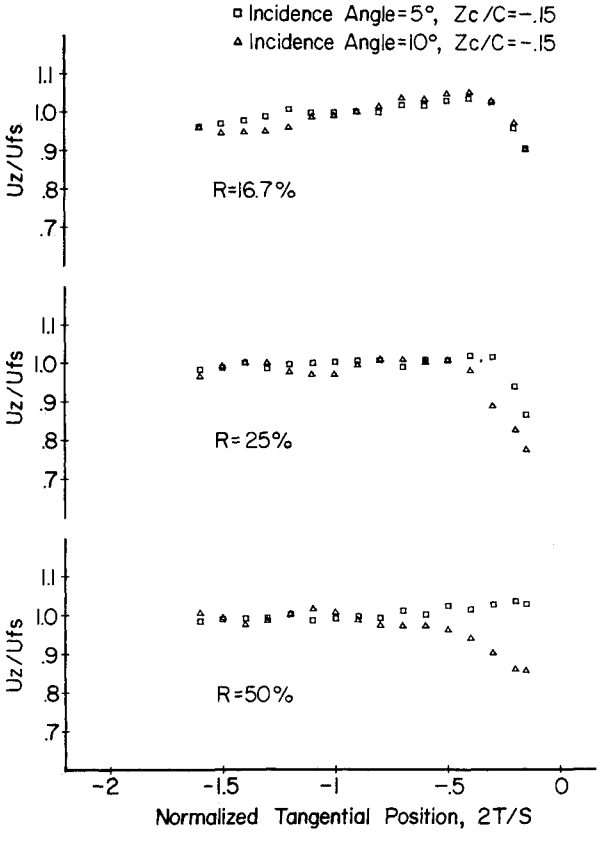

Fig. 9 Variation of the aft-passage axial velocity with incidence for a tip-peaked inlet profile.

For the hub-peaked inlet profile (Fig. 10), again there is no flow separation at 5 deg of incidence. However, the flow appears to be separated from the suction surface at all radial positions at 10 deg of incidence.

Cascade Exit Flowfield

Data describing the effect of inlet velocity profile on the cascade exit region flowfield at 5 deg of incidence are presented in Figs. 11-15. The airfoil is located at $2T/S=0$, with the airfoil suction surface side flowfield corresponding to $2T/S<0$ and the pressure surface side to $2T/S>0$.

At 12.5 span (Fig. 11), the uniform inlet axial wake is symmetric about the airfoil and exhibits the smallest deficit. The wake characteristics associated with the hub-peaked profile are analogous to the uniform profile results but with a somewhat larger wake width and deficit. The tip-peaked inlet profile generated wake is nonsymmetric. The pressure side wake coincides with that for the hub-peaked profile, but the suction side wake coincides with the uniform inlet profile wake. Also, increased radial flows for the tip-peaked profile are evident in the wake region.

At 66.7% span (Fig. 12), the axial wake is symmetric and independent of the inlet velocity profile. The radial velocity in the wake is approximately zero for the uniform and hub-peaked inlet profiles. However, for the tip-peaked inlet profile, wake region radial flow toward the outer span is apparent.

At 83.3% span (Fig. 13), no radial flow is noted in the wake for any of the inlet velocity profiles. However, an inlet velocity profile effect is evident in the axial velocity data. On the airfoil pressure side, the uniform and hub-peaked profile data coincide, whereas on the suction side the uniform and tip-peaked profile data coincide.

The previously noted suction surface flow separation at 10 deg of incidence is also apparent in the cascade exit region. For example, as seen in Fig. 14 at the 16.7, 25, and 50% span positions, the airfoil pressure side data are virtually independent of the incidence angle. However, clear evidence of suction surface flow separation is apparent for the 10-deg incidence angle data.

Wake Profile Similarity

Similarity relations are generally established for the mean velocity wake based on a Gaussian function, as derived from consideration of a two-dimensional isolated flat plate airfoil. Lakshminarayana and Davino[14] presented the coefficients for

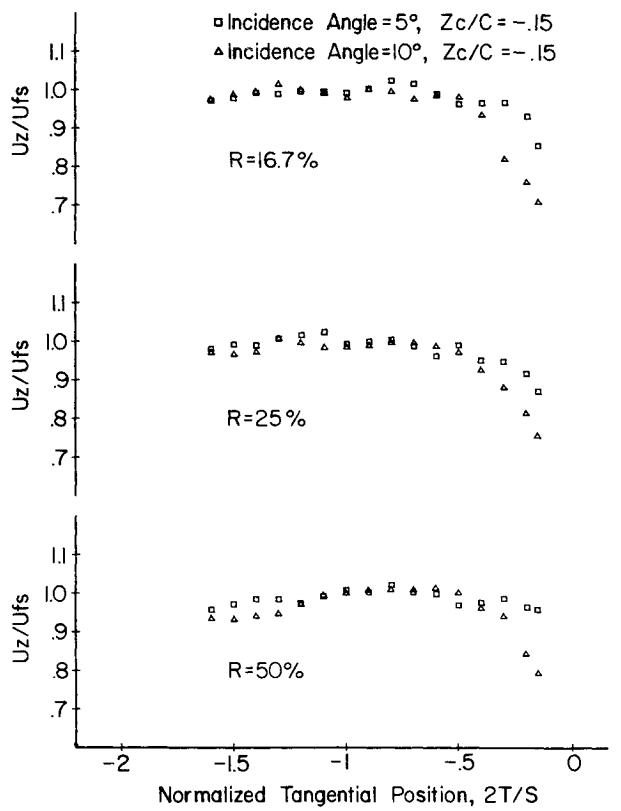

Fig. 10 Variation of the aft-passage axial velocity with incidence for a hub-peaked inlet profile.

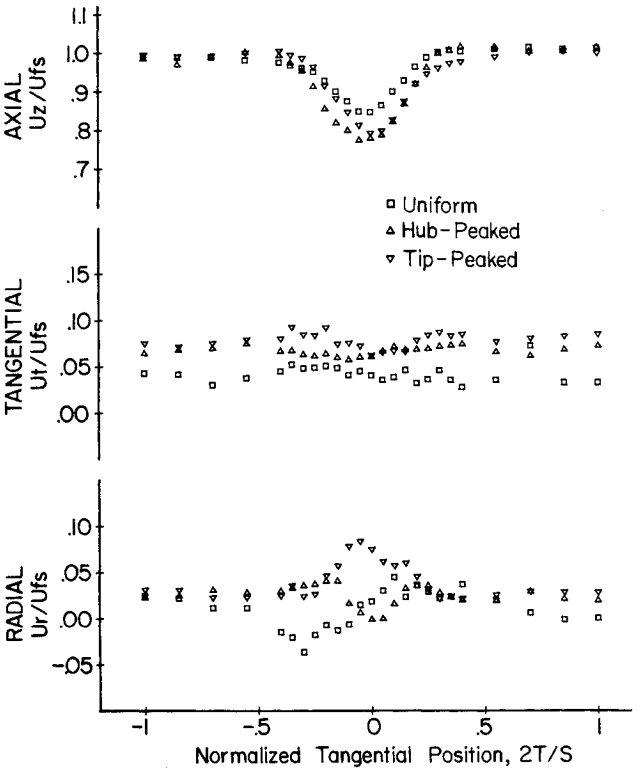

Fig. 11 Cascade exit velocity distributions at $R=12.5\%$ and 5 deg of incidence.

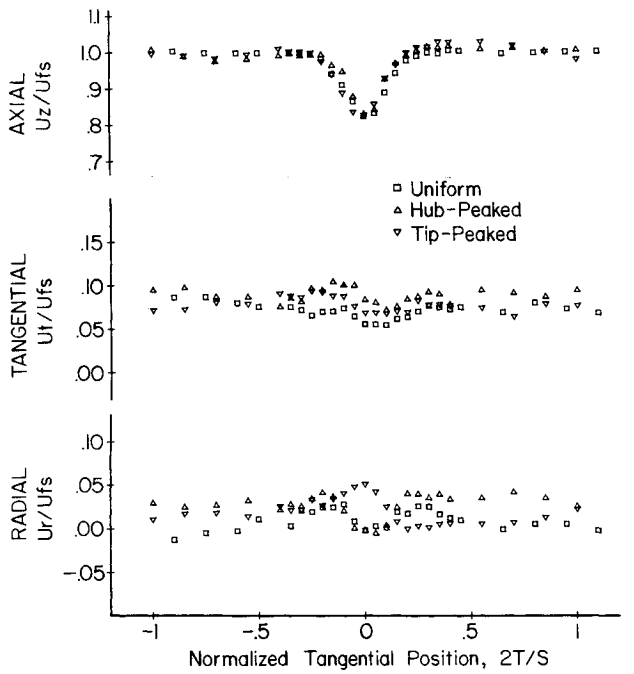

Fig. 12 Cascade exit velocity distributions at $R=66.7\%$ and 5 deg of incidence.

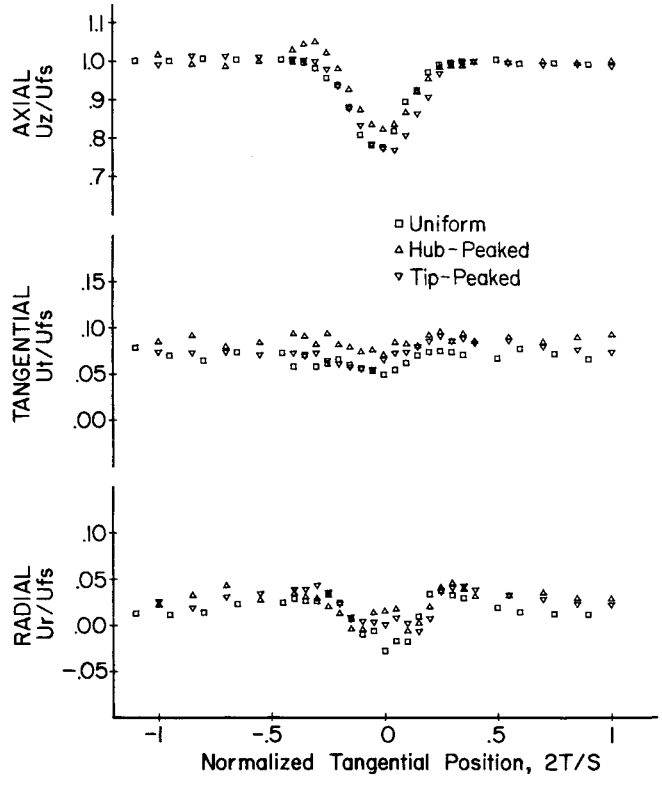

Fig. 13 Cascade exit velocity distributions at $R = 83.3\%$ and 5 deg of incidence.

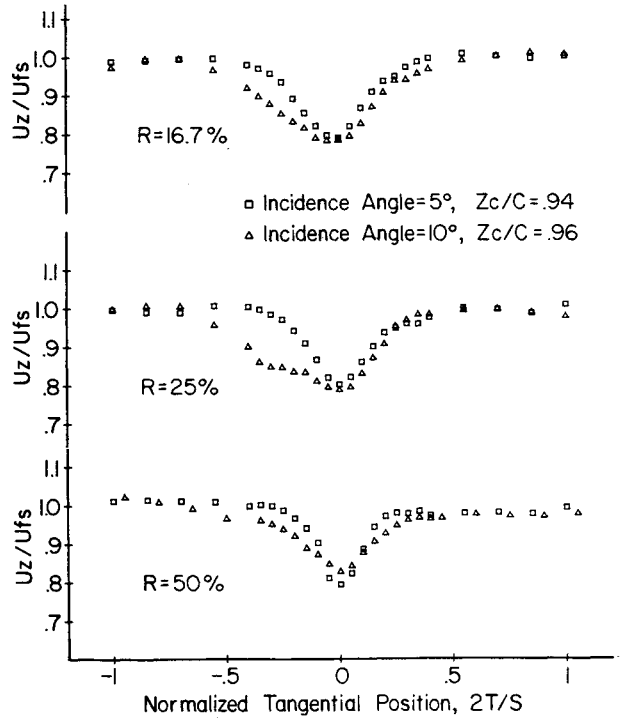

Fig. 14 Variation of the cascade exit axial velocity with incidence for a hub-peaked inlet profile.

the Gaussian similarity function for the velocity deficit as a function of the normalized tangential distance.

$$W/W_{CL} = \exp(-0.693\eta^2) \tag{2}$$

Figure 15 presents the correlation of the exit region data with this similarity relation for the tip-peaked inlet profile at 5 deg of incidence. The correlation is generally good away from

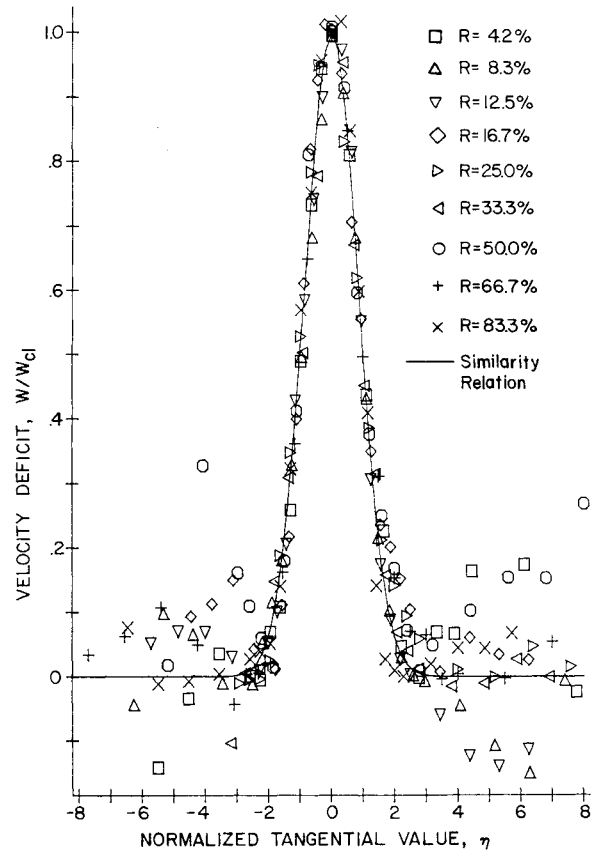

Fig. 15 Similarity of the cascade exit velocity at 5-deg incidence with a tip-peaked inlet profile.

the end-wall regions ($12.5\% < R < 75\%$). Disagreement in the end-wall regions between the data and the similarity function is due to the three-dimensional nature of the flowfield as opposed to the two-dimensionality of the similarity relation. Analogous results were obtained for the hub-peaked and uniform inlet profiles.

VI. Summary and Conclusion

A series of experiments directed at quantifying the effect of inlet velocity profile on the three-dimensional aerodynamic performance of an annular flat plate airfoil cascade have been described. In particular, detailed and extensive data which quantify the airfoil surface pressure distributions, the aft-passage region flow, and the cascade exit region flowfield with a uniform, hub-peaked, and tip-peaked inlet velocity profile at 5 and 10 deg of incidence were obtained. All data were analyzed and correlated with appropriate nonseparated predictions.

1) At an incidence angle of 5 deg, the airfoil surface pressure data exhibit good trendwise correlation with the MERIDL/TSONIC predictions except in regions of flow separation, as expected. Deviations between the data and predictions are probably a result of numerical smoothing effects and of the predictions being inviscid.

2) At an incidence angle of 10 deg, the predictions are in fair qualitative agreement with the data, due to the expected extensive regions of leading-edge flow separation. Quantitative agreement is generally poor.

3) The aft-passage region flowfield data demonstrate the relative uniformity of the freestream region, with the inlet profile affecting primarily the radial velocity component. Also, the suction surface flow separation at 10 deg of incidence was evident.

4) The cascade exit region data quantify the effect of inlet profile on the cascade wakes as a function of radial position.

5) The two-dimensional Gaussian similarity relationship was shown to be appropriate for the wake in the midspan region for each of the inlet profiles. However, in the hub and tip regions, this similarity relationship does not correlate with the wake data due to the increased three-dimensionality of the flowfield.

Acknowledgments

Support of the research reported herein by the NASA-Lewis Research Center, with Mr. Don Boldman serving as technical monitor for the project, is gratefully acknowledged.

References

[1]"Turbomachinery Flow Analysis Methods—Status Report on Maturing Codes," *NASA-Lewis Research Center Conference*, Oct. 1981.

[2]Tesch, W.A. and Pase, R.L., "Design and Performance of a Low Aspect Ratio, High Tip Speed, Multi-Stage Axial Compressor," AIAA Paper 83-1161, June 1983.

[3]Hobbs, D.E. and Weingold, H.D., "Development of Controlled Diffusion Airfoils in Multistage Compressor Applications," ASME Paper 83-GT-211, 1983.

[4]Ecer, A., Akay, H.V., and Sener, B., "A Finite Element Solution of Three-Dimensional Inviscid Rotational Flows Through Curved Ducts," *ASME Symposium on Computation of Internal Flows, FED*, Vol. 14, 1984.

[5]Briley, W.R., McDonald, H., "Three-Dimensional Viscous Flows with Large Secondary Velocity," *ASME Symposium on Computation of Internal Flows, FED*, Vol. 14, 1984.

[6]Kopal, Z., *Numerical Analysis*, Chapman and Hall, London, 1955.

[7]Bergsten, D.E., Stauter, R.C., and Fleeter, S., "Aerodynamic Performance of an Annular Classical Airfoil Cascade," AIAA Paper 83-0179, 1983.

[8]Bryer, D.W. and Pankhurst, R.C., *Pressure-Probe Methods for Determining Wind Speed and Flow Direction*, Her Majesty's Stationery Office, London, 1971.

[9]Sitaram, N., Lakshminarayana, B., and Ravindranath, A., "Conventional Probes for the Relative Flow Measurement in a Turbomachinery Rotor Blade Passage," *ASME Journal of Engineering for Power*, Vol. 103, April 1981, pp. 404-416.

[10]Hinch, D.V. and Fleeter, S., "Hot-Wire Anemometry Measurements of 3-D Mean Velocities in the Purdue Annular Cascade Facility," *ME-TSPC-TR-81-10*, Sept. 1981.

[11]Hall, C.W., *Errors in Experimentation*, Matrix Publishers, Champaign, IL, 1977.

[12]Katsanis, T. and McNally, W.D., "Revised Fortran Program for Calculating Velocities and Streamlines on the Hub-Shroud Midchannel Stream Surface of an Axial-, Radial-, or Mixed-Flow Turbomachine or Annular Duct," NASA TN D-8430 and TN D-8431, 1977.

[13]Katsanis, T., "Fortran Program for Calculating Transonic Velocities on a Blade-to-Blade Stream Surface of a Turbomachine," NASA TN D-5427, 1969.

[14]Lakshminarayana, B. and Davino, R., "Mean Velocity and Decay Characteristics of the Guidevane and Stator Blade Wake of an Axial Flow Compressor," ASME Paper No. 79-GT-9, 1979.